This article has been accepted for publication in a future issue of this journal, but has not been fully edited. Content may change prior to final publication. Citation information: DOI: 10.17775/CSEEJPES.2021.01560, CSEE Journal of Power and Energy Systems

Design And Hardware-In-The-Loop Validation: A Fractional Full Feed-Forward Method Of Grid Voltage In LCL Grid-Connected Inverter System

Qingyi Wang, Binlei Ju, Yudi Lei, Dan Zhou, Shuai Yin, Danyun Li

***Abstract*—The harmonic disturbance in the background grid is a problem that must be considered in the design of a grid-connected inverter. However, the full feed-forward method cannot completely suppress the harmonic disturbance in theory and is sensitive to noise. To tackle these problems, a fractional full feed-forward method of grid voltage is proposed in this paper. Firstly, the mathematical model of the full feed-forward method is deduced, and the difference with the theoretical solution which can suppress all harmonics is analyzed. Then, the parameter equation, the harmonic suppression performance, stability analysis and the implementation process of this method are given. Compared with the full feed-forward method, the proposed method not only further improves the harmonic suppression performance, but also reduces the order of the mathematical model of the differential term in the feed-forward loop. Besides, the proposed method can be used to design feed-forward coefficients flexibly by selecting the order of suppressed harmonics. Finally, the proposed method is validated by a hardware-in-the-loop experiment on the MT real-time control platform NI PXIE-1071.**

***Index Terms*—Full feed-forward method; LCL inverter; Fractional differential; Hardware-in-the-loop.**

+

I. INTRODUCTION

Grid-connected inverter, as a key component connecting renewable energy distributed generation system to the grid, is a research focus at present [1] [2]. LCL grid-connected inverter is widely used in research because of its high-frequency performance, small size, and low cost. Regardless, the stability and quality of grid-connected power should be considered in the design of the LCL grid-connected inverter.

Considering that the voltage at the point of common coupling (PCC) usually contains a large number of harmonics, the output current of the LCL grid-connected inverter will be seriously distorted and cannot meet the requirements of the international standard [3]. LCL grid-connected inverter transmits high-quality electric energy to the grid under the condition of harmonic voltage interference, which is a key factor in the design of a grid-connected inverter. [4][5]. In order to solve the problem, the conventional research includes two methods: One method is to suppress harmonic disturbance by using the advanced controller to replace the original controller; the other method is to suppress harmonic disturbance by increasing a feed-forward loop based on the original controller, which has a faster adjustment speed.

Depending on the different coordinate system, the first method mainly contains repetitive control[6], proportional resonance (PR) control[7], modified proportional-resonant (MPR) control[8], proportional-integral (PI) control[9], PI-Res control[10], as well as the improved forms of the above several methods, etc. Nevertheless, with the continuous improvement of the controller, the control algorithm is more complex, and the parameter design process of the controller is more complicated.

The second method mainly contains the proportional feed-forward method of grid voltage and the full feed-forward method of grid voltage [11] [12] [13]. The proportional feed-forward method can effectively suppress the low-frequency disturbance of grid voltage through a proportional feed-forward link of grid voltage, but cannot suppress the high-frequency disturbance [11]. In order to suppress all the harmonic disturbances in the whole frequency band, the full feed-forward method is usually used in the system [14] [15] [16]. The terms of the full feed-forward method consists of a proportional link, a first-order differential link and a second-order differential link [13]. Even though, it can be seen from the theoretical derivation that the full feed-forward method cannot completely suppress all voltage harmonics. Besides, the first-order and the second-order differential links in the feed-forward loop make the feed-forward loop particularly sensitive to noise, which leads to poor stability of the system.

In order to achieve better control performance, many scholars apply cutting-edge control methods to the inverter control field, such as fuzzy control[17], neural network control[18], robust control[19], fractional-order control and other new controls [20] [21]. Compared with others, the

This work was supported in part by the National Natural Science Foundation of China (No.61703375).

Qingyi Wang (corresponding author, email: wangqingyi@cug.edu.cn), Binlei Ju, Yudi Lei, Dan Zhou, Shuai Yin and Danyun Li are with the School of Automation, China University of Geosciences, and Hubei Key Laboratory of Advanced Control and Intelligent Automation for Complex Systems, Wuhan 430074, China.

fractional-order control is a new control in recent years, where a better control effect and wider application range can be achieved by transforming the integer-order model into the fractional-order model. For example, the fractional-order neural network can achieve better performance for a shunt active power filter (APF) [22], fractional-order sliding mode control is applied in speed regulation of permanent magnet synchronous motor (PMSM) system [23], etc.

According to the discussion above, the full feed-forward method can be further improved. Therefore, based on the theoretical solution of the full feed-forward method, this paper combines the idea of fractional-order control and proposes the fractional-order full feed-forward method. Firstly, the mathematical model of the full feed-forward method and the theoretical solution are analyzed. Then, the fractional-order differential term is approximated to the theoretical solution employing vector, and the parameter design process of the fractional-order full feed-forward method is obtained. Finally, the harmonic suppression performance of several feed-forward methods is analyzed, the effect of this method on the system stability and the implementation process of the fractional-order differential link are also discussed. Compared with the full feed-forward method, the fractional full feed-forward method is closer to the theoretical solution and the differential order of its mathematical model is smaller, which is beneficial for the system to effectively suppress the harmonic disturbance.

The rest of the paper is organized as follows: In Section 2, the mathematical models of the LCL grid-connected inverter system are analyzed. In Section 3, the theoretical derivation process, harmonic suppression performance, stability analysis and implementation process of the proposed method are presented. Section 4 gives the experimental verification and the discussion of the results. The conclusion of this paper is given in Section 5.

II. Mathematical Model of LCL Grid-Connected Inverter System

The structure of the single-phase LCL grid-connected inverter system is shown in Fig. 1. Q_1-Q_4 are the four switches of the inverter respectively. L_1, C and L_2 are the inverter side inductor, the filter capacitor and the grid side inductor respectively. L_g represents the power grid inductor to assume the worst case of power grid impedance. The sampling link of the system is implemented by the zero-order holder (ZOH), and the modulation method of the system is sinusoidal pulse width modulation (SPWM). Also, the control strategy of the system adopts the double current loop control of the grid-connected current i_2 and the current i_c flowing through C. On the one hand, it can guarantee the rapidity of the system control; on the other hand, it can guarantee the stable operation of the system by increasing the damping of the system.

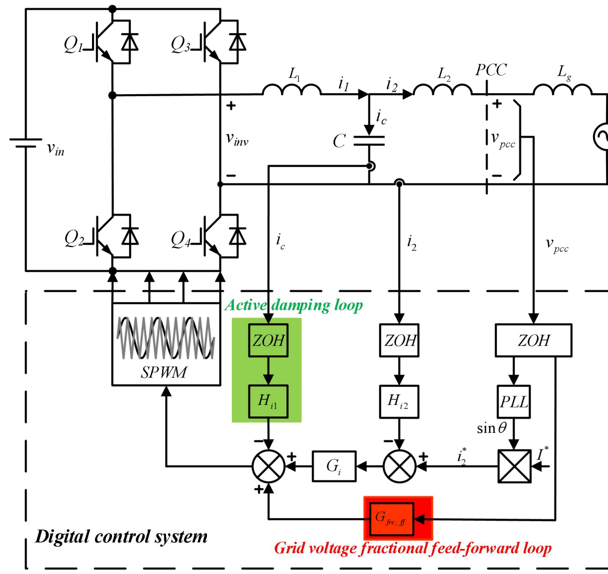

Fig. 1. *The structure of single-phase LCL grid-connected inverter system.*

Figure. 2 shows the control block diagram of the LCL grid-connected inverter system. As can be seen from Fig. 2, the control block diagram of the digital system mainly includes the current controller $G_i(s)$ with the sampling coefficient H_{i2} of $i_2(s)$, the active damping loop with the sampling coefficient H_{i1} of i_c, the digital delay $G_d(s)$, the modulation gain K_{PWM}, and the LCL filter $G_{LCL}(s)$.

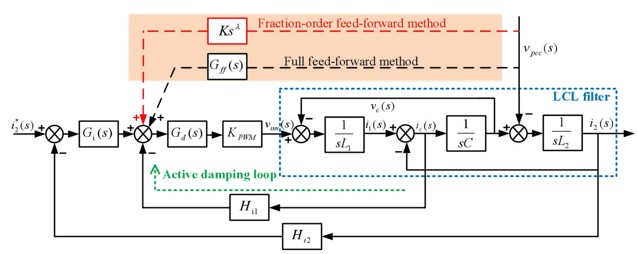

Fig. 2. *Control block diagram of LCL grid-connected inverter system.*

The blue box in Fig. 2 is the transfer block diagram of the LCL filter, the open-loop transfer function of the LCL filter can be expressed as the relation between the inverter side voltage $v_{inv}(s)$ and $i_2(s)$

$$G_{LCL}(s) = \frac{i_2(s)}{v_{inv}(s)} = \frac{1}{s^3 L_1 L_2 C + s(L_1 + L_2)} \tag{1}$$

$G_i(s)$ is a PR controller with a well-behaved tracking effect on a specific frequency signal. Its mathematical model is set as

$$G_i(s) = K_p + \frac{2K_r \omega_i s}{s^2 + 2\omega_i s + \omega_0^2} \tag{2}$$

where K_p and K_r are the proportionality coefficient and resonance coefficient respectively. ω_i reflects the bandwidth of the PR controller, and ω_o represents the angular frequency of the fundamental wave. In this paper, $\omega_0 = 100\pi rad/s$.

$G_d(s)$ represents the system delay of $1.5T_s$ including a sampling delay of $0.5T_s$ caused by ZOH and T_s delay caused by PWM modulation and calculation, where T_s is the sample time.

$$G_d(s) \approx e^{-1.5sT_s} \tag{3}$$

The active damping loop of i_c (the green line loop) in Fig.2 can be equivalent to the virtual impedance $Z_{eq}(s)$ in parallel to C.

$$Z_{eq}(s) = \frac{v_c(s)}{i_c(s)} = \frac{L_1}{CH_{i1}K_{PWM}G_d(s)} \tag{4}$$

To sum up, the open-loop transfer function of the system $H(s)$ in Fig. 2 can be obtained,

$$H(s) = \frac{H_{i2}G_i(s)K_{PWM}G_d(s)}{sL_1(L_2+L_g)C} \cdot \frac{1}{s^2 + \frac{1}{CZ_{eq}(s)}s + \omega_r^2} \tag{5}$$

where $K_{PWM} = v_{inv}/v_{tri}$ is the modulation gain, v_{tri} is the triangular carrier, and $\omega_r = 2\pi f_r = \sqrt{\frac{L_1+L_2}{L_1L_2C}}$ is the resonant angular frequency of the LCL filter.

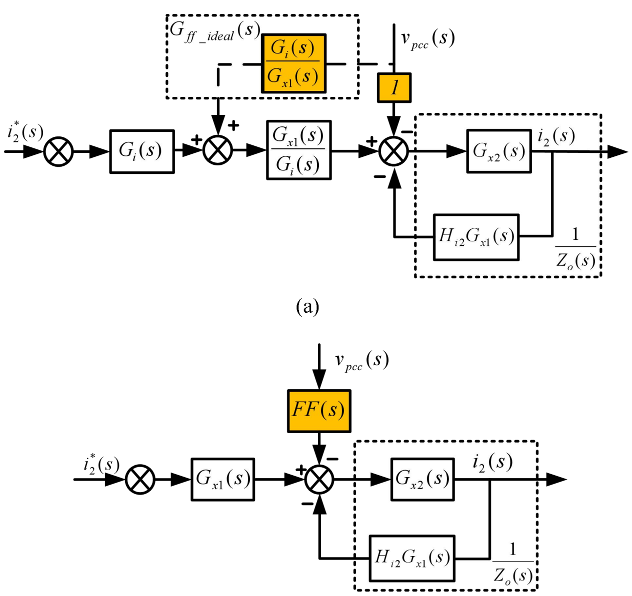

(a)

(b)

Fig. 3. *Control block diagram of the system with ideal full feed-forward method. (a) Actual implementation form; (b) Equivalent transformation form.*

Analyzing Fig. 2 from the perspective of disturbance, it is obvious that the disturbance of the system is the PCC terminal voltage $v_{pcc}(s)$. In order to suppress the voltage harmonic disturbance caused by $v_{pcc}(s)$, the traditional full feed-forward method is used. Hence, the control block diagram of the system can be transformed to Fig. 3. The transfer functions of $G_{x1}(s)$ and $G_{x2}(s)$ are given in:

$$\begin{aligned} G_{x1}(s) &= \frac{G_i(s)K_{PWM}G_d(s)}{s^2CL_1 + sCH_{i1}K_{PWM}G_d(s)+1} \\ G_{x2}(s) &= \frac{s^2L_1C + sCH_{i1}K_{PWM}G_d(s)+1}{s^3L_1CL_2 + s^2H_{i1}K_{PWM}G_d(s)CL_2 + s\left(L_1+L_2\right)} \end{aligned} \tag{6}$$

The dotted box in Fig. 3 (a) represents the ideal full feed-forward loop of grid voltage, according to Eq. (2) and Eq. (6), the ideal full feed-forward transfer function $G_{ff\_ideal}(s)$ can be expressed as

$$G_{ff\_ideal}(s) = \frac{G_i(s)}{G_{x1}(s)} = \frac{s^2L_1C}{K_{PWM}G_d(s)} + sCH_{i1} + \frac{1}{K_{PWM}G_d(s)} \tag{7}$$

As the feed-forward loop is added to the system, the influence coefficient of the feed-forward control is $FF(s)$,

$$FF(s) = 1 - \frac{G_{ff}(s)}{G_i(s)}G_{x1}(s) \tag{8}$$

where $G_{ff}(s)$ represents the transfer function of different feed-forward methods.

By comparing Fig. 3(a) and (b), it is obvious that $FF(s)=1$ (as shown in Fig. 3(a)) when the system runs without feed-forward method, and the grid harmonics in PCC can directly interfere with the operation of the system. However, when $G_{ff\_ideal}(s)$ is used in the system, $FF(s)=0$ (as shown in Fig. 3(b)), and the grid harmonics will not cause interference to the system.

Even though $FF(s)$ is infinitely close to 0 with $G_{ff\_ideal}(s)$, and the interference of $v_{pcc}(s)$ to the system can be eliminated. But in fact, $\frac{1}{G_d(s)}$ is an advanced link and cannot be implemented in the digital system. Therefore, the transfer function of the traditional full feed-forward method is

$$G_{ff}(s) = \frac{s^2L_1C}{K_{PWM}} + sCH_{i1} + \frac{1}{K_{PWM}} \tag{9}$$

Eq. (9) can be implemented in a digital system. However, there is still a problem, that is, the 2-order differential term in Eq. (9) is very sensitive to noise, which makes it difficult for the system to run stably for a long time.

$$G_{ff\_p}(s) = \frac{1}{K_{PWM}} \tag{10}$$

Usually in engineering practice, the system is generally controlled by current loop PR controller combined with the proportional feed-forward feedback (as shown in Eq. (10)). Compared with Eq. (9), Eq. (10) has a poor suppression effect on high frequency harmonics, but the control process of Eq. (10) is simpler and ensures the stability of the system.

This article has been accepted for publication in a future issue of this journal, but has not been fully edited. Content may change prior to final publication.
Citation information: DOI: 10.17775/CSEEJPES.2021.01560, CSEE Journal of Power and Energy Systems

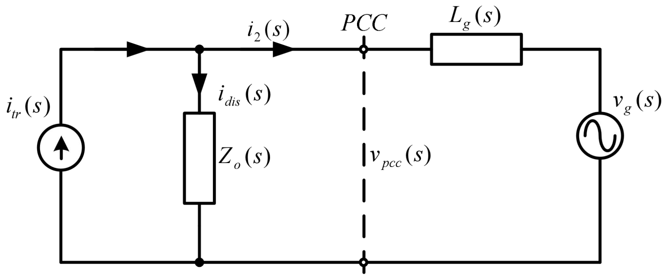

Fig. 4. *Equivalent Norton circuit model.*

Considering that it is not very simple and clear to use $FF(s)$ to describe the harmonic suppression in an actual system, and it cannot reflect the overall performance of the system. Therefore, based on $FF(s)$, this paper adopts the form of the system equivalent output impedance $Z_o(s)$ in Fig. 4 to visually describe the suppression effect of the system on the power grid harmonics.

Figure. 4 shows the equivalent Norton circuit of the system. For the convenience of analysis, v_{in} is transformed into the current source i_{tr}, and i_{dis} represents the current flowing through $Z_o(s)$. According to Fig. 4, the relationship between i_2, i_{tr} and v_g can be expressed as

$$i_2(s) = \frac{Z_o(s)}{Z_o(s)+L_g(s)} i_{tr}(s) - \frac{1}{Z_o(s)+L_g(s)} v_g(s) \tag{11}$$

According to Eq. (11), the effect of v_g on i_2 is negatively correlated with the size of $Z_o(s)$ and L_g. Since the size of L_g is determined by the actual grid, the harmonic effect of the grid can be weakened by increasing $Z_o(s)$.

Combined with Fig. 3(b) and Fig. 4, the transfer function between $v_{pcc}(s)$ and i_2 can be expressed as $\frac{1}{Z_o(s)}$, where $Z_o(s)$ is the equivalent output impedance of the system without feed-forward method,

$$\begin{aligned} Z_o(s) = \frac{v_{pcc}(s)}{i_2(s)} &= sL_2 + \frac{sL_1}{s^2L_1C + sCH_{i1}K_{PWM}G_d(s)+1} \\ &+ \frac{G_i(s)H_{i2}K_{PWM}G_d(s)}{s^2L_1C + sCH_{i1}K_{PWM}G_d(s)+1} \end{aligned} \tag{12}$$

and the equivalent output impedance of the ideal full feed-forward method is changed to $Z_o^{\sim}(s)$.

$$Z_o^{\sim}(s) = \frac{v_{pcc}(s)}{i_2(s)} = \frac{Z_o(s)}{FF(s)} \tag{13}$$

III. The Proposed Fractional-Order Full Feed-Forward Method of Grid Voltage

It can be seen from Eq. (7) and Eq. (9) that the traditional full feed-forward method mainly has two shortcomings. First, the traditional full feed-forward method is usually used to approximate $G_{ff\_ideal}(s)$ over the entire frequency range. This method can offset most of the grid voltage harmonic interference, but cannot completely cancel it. Secondly, because there is a 2-order differential term in Eq. (9), which may cause over-modulation and thus affect the suppression effect of the feed-forward link on harmonics. Therefore, instead of approximating $G_{ff\_ideal}(s)$ within the whole frequency range, this paper uses fractional order differential term to approximate $G_{ff\_ideal}(s)$ at a specific frequency, so as to realize the suppression of the harmonic interference of the grid voltage within a certain frequency range.

A. The Mathematical Model and parameter design process of Fractional-order Full Feed-Forward Method

In order to further analyze $G_{ff\_ideal}(s)$, $s = \omega e^{j\frac{\pi}{2}}$ and Euler's formula ($e^{jx} = \cos x + j\sin x$) are substituted into Eq. (7), and Eq. (7) is split into real and imaginary parts, as shown in Eq. (14).

$$\begin{aligned} &\text{x-axis: } \frac{1-\omega^2L_1C}{K_{PWM}}\cos(1.5\omega T_s) \\ &\text{y-axis: } \omega CH_{i1} + \frac{1-\omega^2L_1C}{K_{PWM}}\sin(1.5\omega T_s) \end{aligned} \tag{14}$$

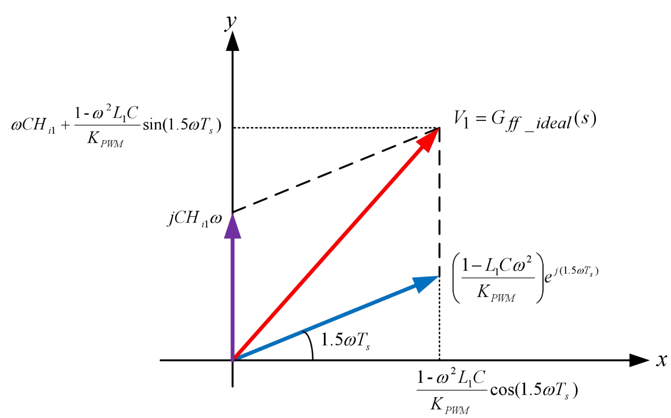

Fig. 5. *Vector diagrams of* $G_{ff\_ideal}(s)$.

The vector of $V_1 = G_{ff\_ideal}(s)$ are drawn in Fig. 5, in which the purple vector(fixed vector) and the blue vector (rotation vector) are the constituent vectors obtained by substituting $s = \omega e^{j\frac{\pi}{2}}$ in Eq. (7), and the real part and imaginary parts in Eq. (14) are marked on the x-axis and y-axis.

According to the equations marked in Fig. 5, it can be seen that because of the existence of $e^{j(1.5\omega T_s)}$ in the blue vector, the blue vector is a rotation vector. Therefore, V_1 is also rotating,

According to Eq. (14), the magnitude and angle of V_1 can be expressed as

$$\begin{aligned}&|V_1| = \sqrt{\left(\frac{a}{K_{PWM}}\right)^2 + b^2 + \frac{2ab}{K_{PWM}}\sin(1.5\omega T_s)}\\ &\angle V_1 = \arctan\left(\frac{K_{PWM}b + a\sin(1.5\omega T_s)}{a\cos(1.5\omega T_s)}\right)\\ &a = 1 - L_1C\omega^2 \quad b=\omega CH_{i1}\end{aligned} \tag{15}$$

According to Eq. (15), the independent variables of magnitude and angle are both angular frequency ω, and the relationship is not linear, so it is difficult to approximate V_1 directly.

In this paper, the fractional full feed-forward method V_2 is used to approximate V_1 at a particular ω. The transfer function of V_2 is expressed as

$$\begin{aligned}&V_2 : G_{frc\_ff}(s) = Ks^{\lambda}\\ &|V_2| = K\omega^{\lambda}, \angle V_2 = \frac{\lambda\pi}{2}\end{aligned} \tag{16}$$

where $s^{\lambda} = (j\omega)^{\lambda} = \omega^{\lambda}e^{j\frac{\lambda\pi}{2}}$.

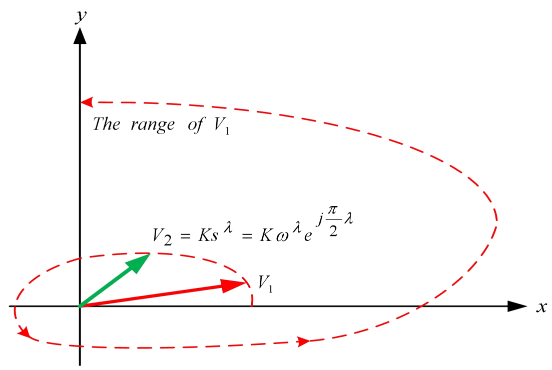

Fig. 6. *Approximation of the vectors V_1 and V_2.*

As can be seen from Fig. 6, the red dotted line represents the motion trajectory of V_1 as ω increases, and the solid green line represents V_2. When V_2 coincides with a certain state in the motion trajectory of V_1, the approximation process of $G_{ff\_ideal}(s)$ is completed.

According to Eq. (15) and Eq. (16), the fractional order λ and the gain K can be calculated as below, where $\lambda \in (0,2)$ and $\omega \in (0, \pi f_s)$.

$$\begin{aligned}&\lambda = \frac{2}{\pi}\arctan\left(\frac{K_{PWM}b + a\sin(1.5\omega T_s)}{a\cos(1.5\omega T_s)}\right)\\ &K = \frac{1}{\omega^{\lambda}}\sqrt{\left(\frac{a}{K_{PWM}}\right)^2 + b^2 + \frac{2ab}{K_{PWM}}\sin(1.5\omega T_s)}\end{aligned} \tag{17}$$

It can be seen from Eq. (17) that, when L_1, C and H_{i1} have been determined, λ and K are two functions only related to ω. By substituting $\omega_h = \omega_0 N = 100\pi N$ into Eq. (17), the independent variable is changed from ω_h to N, where ω_h is the harmonic angular frequency, and N represents the order of the harmonic we want to suppress.

In order to show the suppression effect of the proposed method obviously, the influence coefficient of the proposed method $FF_{frc}(s)$ is expressed as

$$FF_{frc}(s) = 1 - G_{frc-ff}(s)\frac{G_{x1}(s)}{G_i(s)} \tag{18}$$

where $FF_{frc}(s) \approx FF(s)|_{s=j\omega_h}$.

B. Analysis of Harmonic Suppression Performance

Table 1 Mathematical models of several feed-forward methods

Feed-forward method	Mathematical model
Type 1	$G_{ff\_p}(s) = \frac{1}{K_{PWM}}$
Type 2	$sCH_{i1} + \frac{1}{K_{PWM}}$
Type 3	$G_{ff}(s) = \frac{s^2L_1C}{K_{PWM}} + sCH_{i1} + \frac{1}{K_{PWM}}$
N=5 (the proposed method)	$G_{frc-ff}(s) = 0.0252s^{0.1012}$
N=7 (the proposed method)	$G_{frc-ff}(s) = 0.0169s^{0.1431}$

The Bode plot of Eq. (8), Eq. (9), Eq. (10) and Eq. (18) is given in Fig. 7 to further indicate the suppression effect of different feed-forward methods on harmonic disturbances. As can be seen from Table 1, the four feed-forward methods are $G_{ff\_p}(s)$, $G_{ff}(s)$, the simplified form of $G_{ff}(s)$ (only include the proportional link and the 1-order differential link), and $G_{frc-ff}(s)$, In which $G_{frc-ff}(s)$ is approximated as a 5th model, and the implementation process of $G_{frc-ff}(s)$ would be explained in detail in Section 3. D.

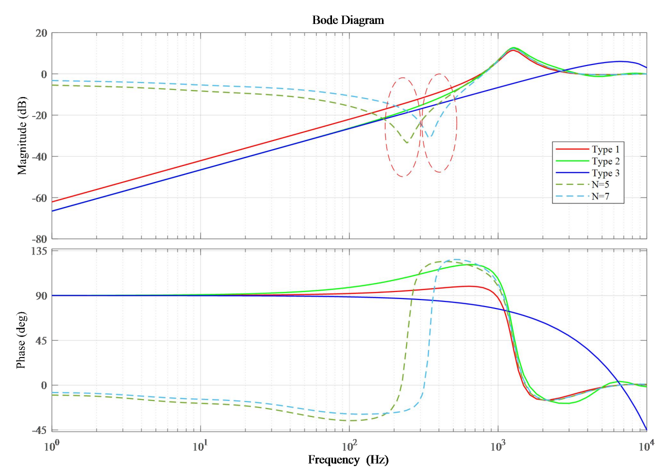

Fig. 7. *Bode diagram of the influence coefficient of different feed-forward controls.*

First, three traditional feed-forward methods of Type 1, Type 2 and Type 3 are analyzed. The characteristics of Type 1, Type 2 and Type 3 are similar in the low-frequency band. In the range of middle and high-frequency bands, the amplitude-frequency characteristics of Type1 and Type2 are similar and both are higher than that of Type3. Therefore,

This article has been accepted for publication in a future issue of this journal, but has not been fully edited. Content may change prior to final publication.
Citation information: DOI: 10.17775/CSEEJPES.2021.01560, CSEE Journal of Power and Energy Systems

Type3 has a stronger harmonic suppression ability in the middle and high-frequency bands.

Then, compared with Type1, Type 2 and Type 3 in Fig. 6, the amplitude of the proposed method is lower around a particular frequency, such as the amplitude of N=5 around $250Hz$ and the amplitude of N=7 around $350Hz$. Since the amplitude in Fig. 7 is positively correlated with the degree of harmonic interference. It can be seen that the proposed method can effectively suppress the harmonics around a specific frequency point.

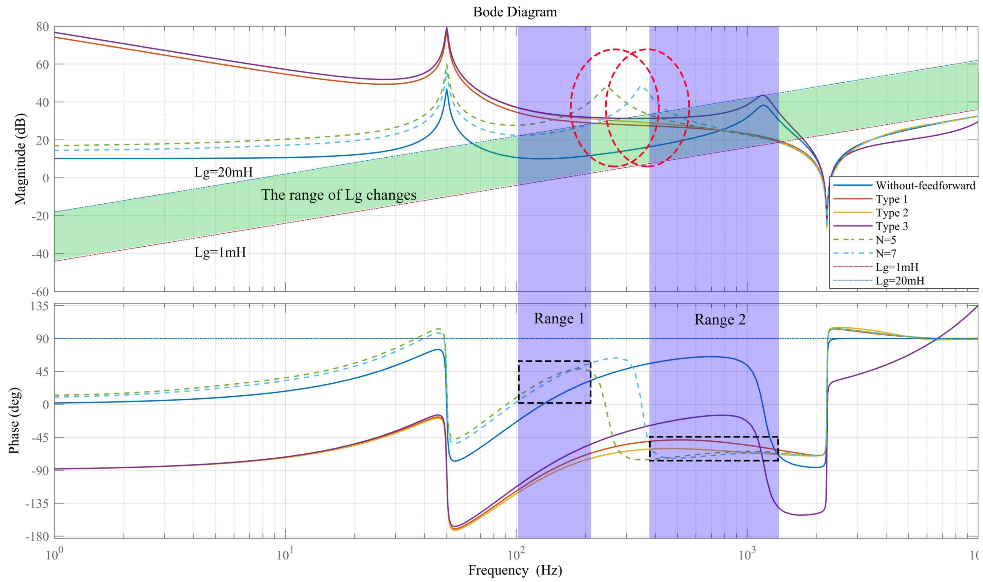

Fig. 8. *Bode diagram of the equivalent output impedance of system with different feed-forward control.*

By comparing the four feed-forward methods in Fig. 8, it can be seen that the proposed method differs greatly from the three methods of Type1, Type2 and Type3 in the low-frequency bands. Considering that there is almost no DC component in the grid, the low-frequency characteristics of the several methods have little influence on the THD of the grid-connected power. Therefore, the influence in the low-frequency band ($<50Hz$) will not be analyzed.

The harmonic suppression performance of the proposed method is mainly reflected in the middle frequency band. It can be seen that the proposed method has a new amplitude-frequency peak of $Z_o^{\sim}(s)$ near the selected frequency point, and the phase frequency characteristic has a downward jump. Therefore, the ability to suppress the harmonics in the specific frequency band is enhanced. Moreover, the position of the impedance peak is determined N , and the selection range of N is $1<N<\dfrac{f_s}{2*50}$ when $\lambda\in(0,2)$. In order to ensure that the differential action of the proposed method is weak, the upper limit at $\lambda=1$ is $N=\dfrac{1}{200\pi}\sqrt{\dfrac{1}{L_1C}}$.

In order to analyze the stability of the proposed method under weak grid, the green shaded part in Fig. 8 shows the possible variation range of L_g , and the blue shaded part corresponds to the phase curve range when $\left|Z_o^{\sim}(s)\right|=\left|L_g(s)\right|$. And the basis to judge the stability of the system under the condition of grid impedance change is first given: when $\left|Z_o^{\sim}(s)\right|=\left|L_g(s)\right|$, if the angle between the two is close to 180° , $Z_o^{\sim}(s)+L_g(s)=0$, which can be seen that the system cannot operate stably according to Eq.(11).

The analysis of Range 1 and Range 2 shows that, the phase curve of the proposed method in range 1 is close to 90°, while that in range 2 is close to -90°. Therefore, the stability of the proposed method mainly depends on range 2. In order to ensure that the proposed method has good stability, the stability constraint conditions of the corresponding parameter design in Range 2 can be given by combining the above system stability judgment methods.

$$\angle Z_o^{\sim}(s)>-90^o\ |_{s=jN\omega_0} \tag{19}$$

Summarizing the above analysis, the following conclusions can be drawn: when $f<50N$, the frequency characteristics of the proposed method are close to Without feed-forward. Around $f=50N$, the new impedance peak can effectively suppress the harmonic disturbance of the grid, while the phase curve jump. when $f>50N$, the frequency characteristics of the proposed method are close to Type1. Therefore, the proposed method can be regarded as a method switching between Without feed-forward and Type 1, which can effectively suppress the harmonic interference around the switching frequency point.

C. Root locus analysis of the system using the proposed method

In this part, the Z-domain root locus analysis is used to verify the effectiveness of the proposed method in the digital control system.

According to Eq. (11), the mathematical model of the system using the proposed method can be transformed into the following form.

$$i_2(s)=\frac{Z_o^{\sim}(s)}{Z_o^{\sim}(s)+L_g(s)}\left(i_{tr}(s)-\frac{v_g(s)}{Z_o^{\sim}(s)}\right) \tag{20}$$

Considering that the system can operate stably under the condition of a strong grid ($L_g(s)=0$), so the stability of the system under a weak grid depends on whether $N(s)$ is stable.

$$N(s)=\frac{1}{1+\dfrac{L_g(s)}{Z_o^{\sim}(s)}} \tag{21}$$

where $N(s)$ is equivalent to a closed-loop negative feedback transfer function, and the characteristic root equation is

$$1+L_g(s)\frac{F(s)}{Z_o(s)}=0 \tag{22}$$

Therefore, the root locus curve in the Z domain can be obtained by discretizing Eq. (21). In the discrete model of the system, the sampled signals are discretized by ZOH transform, while $G_i(s)$ and $G_{frc\_ff}(s)$ are discretized by Tustin transform.

The system root locus of the proposed method with different N is shown in Fig. 9. The gain of the root locus reflects the size of L_g. As L_g increases in Fig. 9, the root locus of the system moves from the inside of the unit circle to the outside, and the larger the N is, the closer the corresponding system root locus is to the outside of the unit circle. Therefore, when L_g changes, the system runs conditionally stably, but the larger L_g is, the worse the system stability is. In addition, the larger the N is, the larger the order λ of the differential term is, so the more difficult the system is to operate stably.

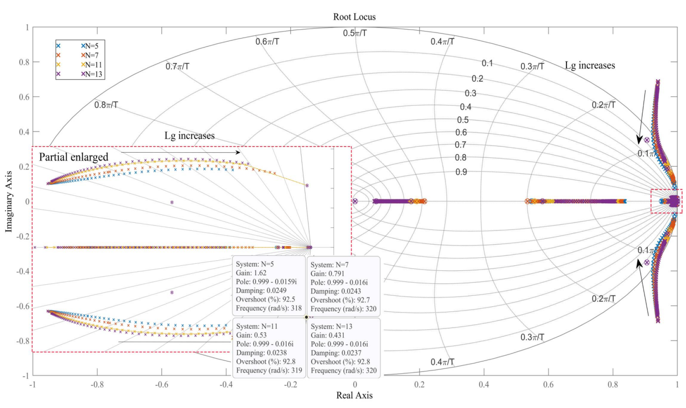

Fig. 9. *The system root locus of the proposed method.*

D. Discrete time-domain model of fractional full feed-forward method

Since the fractional differential term cannot be implemented directly, the approximation method of the higher-order integer term is usually to implement the fractional differential term. The implementation of the fractional-order continuous model in the digital system includes two steps: the discrete and the integer-order approximation.

Firstly, this paper uses an improved Tustin transform to discrete the fractional-order operator,

$$s^{\lambda}=\alpha^{\lambda}\left(\frac{1-z^{-1}}{1+z^{-1}}\right)^{\lambda} \tag{23}$$

where $\alpha=\dfrac{\omega_c}{\tan(\frac{\omega_c T_s}{2})}$, and ω_c is the cutoff frequency.

Then, the Taylor series is used to approximate the fractional-order operator s^{λ}, according to the method proposed from the literature [24], let $z=\omega^{-1}$ to ensure that the differential link is causal, Eq. (22) can be written as

$$\alpha^{\lambda}\left(\frac{1-\omega}{1+\omega}\right)^{\lambda}=\alpha^{\lambda}\sum_{k=0}^{n}f_k(\lambda)\omega^k\ ,|\omega|<1 \tag{4}$$

where n is the number of the Taylor expansion, and $f_k(\beta)$ is the k-order derivative term of the Taylor expansion, which is given as:

$$f_k(\lambda)=\frac{1}{k!}\frac{\mathrm{d}^k}{\mathrm{d}\omega^k}\left(\frac{1-\omega}{1+\omega}\right)^{\lambda}\Bigg|_{\omega=0} \tag{25}$$

Substituting Eq. (23), (24) and (25) into Eq. (16), the output of $G_{frc}(z)$ can be obtained as

$$G_{frc}(z)=\left[K\alpha^{\lambda}\sum_{k=0}^{n}f_k(\lambda)\omega^k\right]v_{pcc}(z) \tag{26}$$

where $v_{pcc}(z)$ represents the ZOH-sampling PCC voltage. In order to better match the implementation form in the digital system, Eq. (25) can be transformed into Eq. (26),

$$\begin{aligned}G_{frc}(k)=K\alpha^{\lambda}[v_{pcc}(k)+f_1(\lambda)v_{pcc}(k-1)+\ldots\\+f_{n-1}(\lambda)v_{pcc}(k-(n-1))+f_n(\lambda)v_{pcc}(k-n)]\end{aligned} \tag{27}$$

Generally, the 5th order model has a good approximation effect to the fractional link, so $n=5$ is used in this paper, and the approximate frequency range is selected as $(1, f_s/2)$.

IV. HARDWARE-IN-THE-LOOP EXPERIMENTAL RESULTS AND ANALYSIS

In order to verify the effectiveness of the proposed fractional full feed-forward method, the LCL grid-connected inverter system is established. The system parameters are shown in Table 2, and the experiment platform is shown in Fig. 10. The control method is implemented by using NI PXIE-1071, and the THD of the output grid side current is measured by the power analyzer.

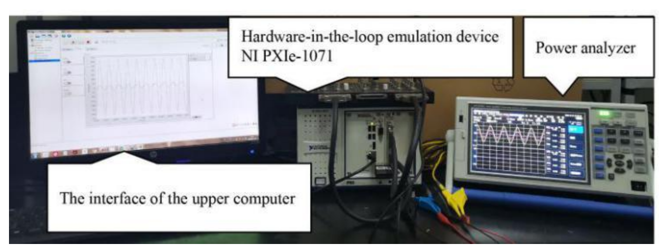

Fig. 10. *Hardware-in-the-loop experiment hardware configuration.*

As shown in Fig. 10 and Fig. 11, NI PXIE-1071 mainly realizes the hardware-in-the-loop simulation function by HIL software. The power circuit of the system is implemented by

This article has been accepted for publication in a future issue of this journal, but has not been fully edited. Content may change prior to final publication. Citation information: DOI: 10.17775/CSEEJPES.2021.01560, CSEE Journal of Power and Energy Systems

the FPGA board of NI PXIE-1071. The sampling and control circuit is converted into C program through the NI standard C language code generation of Simulink, and is loaded into the control board of NI PXIE-1071. The experimental results are displayed on the power analyzer by connecting an external port board connected to a series of ports defined inside the NI PXIE-1071.

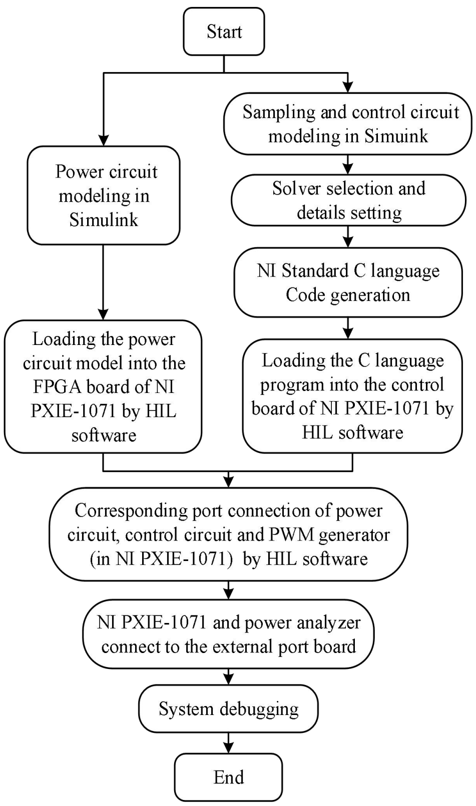

Fig. 11. *Operation flow chart of NI PXIE-1071.*

Table 2 System parameter table

Parameter	Value	Parameter	Value
v_{in}	$360V$	L_1	$2mH$
v_g	$220V$	L_2	$0.7mH$
P_{out}	$6kW$	C	$10\mu F$
f_0	$50Hz$	f_{switch}	$10kHz$
f_s	$20kHz$	H_{i1}	0.14
H_{i2}	0.15	R_{in}	0.1Ω
K_p	1.2	K_r	80
L_g	$1\mu H$	v_{tri}	20

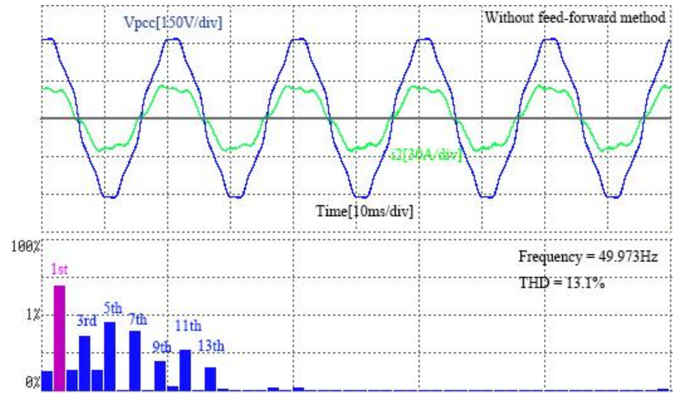

Fig. 12. *Grid-connected voltage-current waveform and current harmonic analysis without feed-forward method.*

In order to simulate the existence of harmonics in the background grid, a series of 5^{th}, 7^{th}, 11^{th} and 13^{th} harmonics are injected into the PCC terminal, and the THD of v_{pcc} is 6.6%. Fig. 12 shows the output waveform of the system without the feed-forward method. It can be seen that the THD of i_2 is 13.1%, which cannot meet the grid side current standard within 5%. Therefore, an additional grid voltage feed-forward method is needed to suppress harmonic interference.

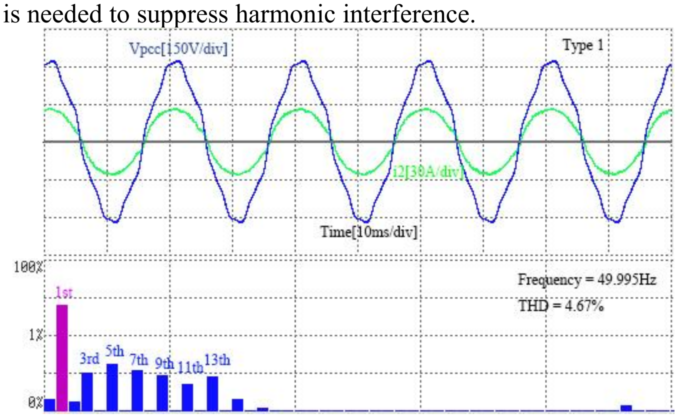

(a) Type 1.

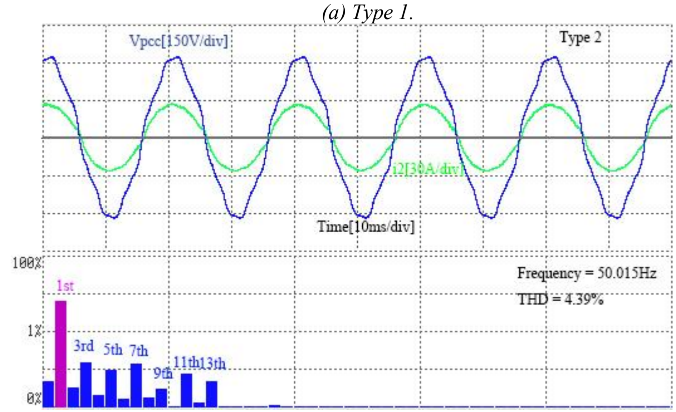

(b)Type 2.

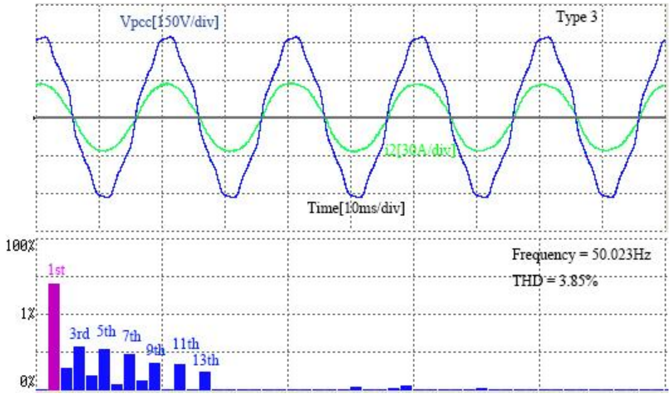

(c)Type 3.

Fig. 13. *Grid-connected voltage-current waveform and current harmonic analysis with traditional feed-forward methods.*

As can be seen from Fig. 13, $G_{ff\_p}(s)$ is used in Fig. 13 (a), $G_{ff}(s)$ and its simplified form is used respectively in Fig. 13 (b), (c) to further offset the disturbance of background harmonics. Obviously, the waveform of i_2 is close to the sine wave, and the THD decreases from 4.67% (in Fig. 13 (a)) to 4.39% (in Fig. 13 (b)) and 3.85% (in Fig. 13 (c)) with the gradual completion of the full feed-forward term. The results in Fig. 13 are consistent with the analysis in Fig. 7 and Fig. 8.

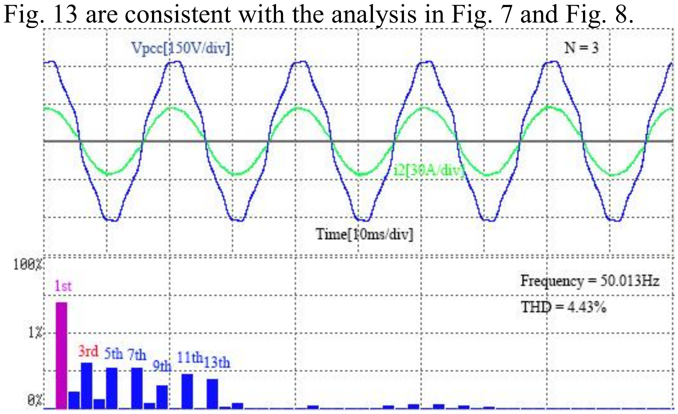

(a) $N = 3$: $G_{frc-ff}(s) = 0.0362s^{0.0603}$.

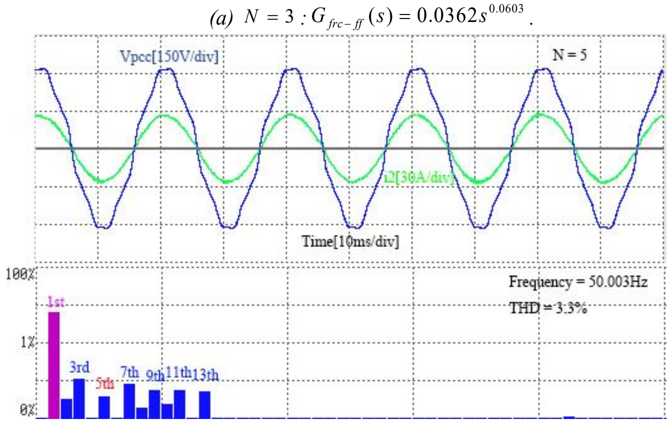

(b) $N = 5$: $G_{frc-ff}(s) = 0.0252s^{0.1012}$.

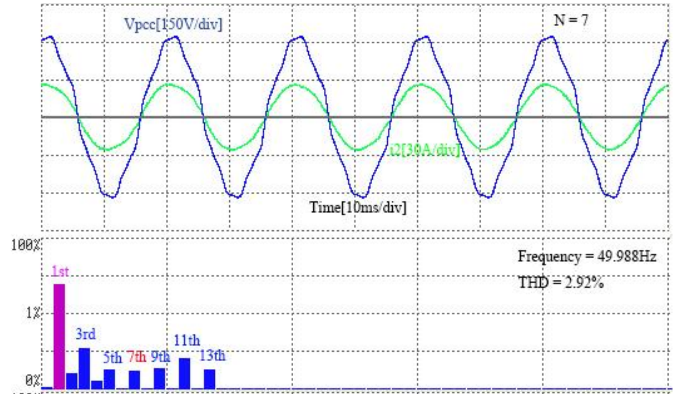

(c) $N = 7$: $G_{frc-ff}(s) = 0.0169s^{0.1431}$.

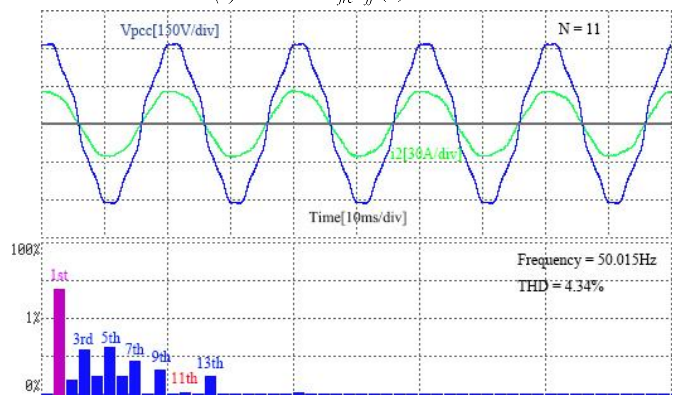

(d) $N = 11$: $G_{frc-ff}(s) = 0.0066s^{0.2331}$.

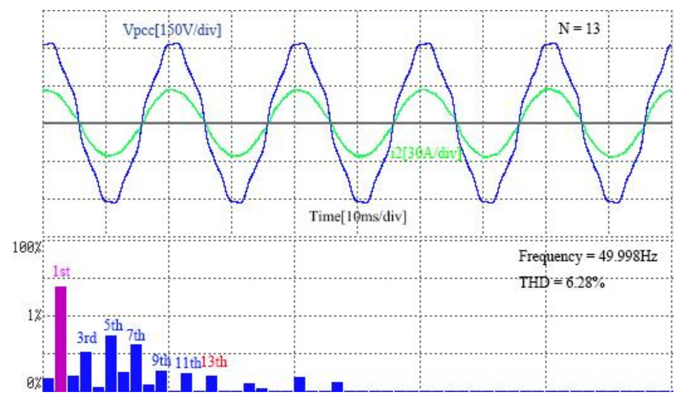

(e) $N = 13$: $G_{frc-ff}(s) = 0.0037s^{0.284}$.

Fig. 14. *Grid-connected voltage-current waveform and current harmonic analysis of the proposed method with different control parameters.*

In Fig. 14, the proposed method with different control parameters is used, and the corresponding feed-forward loop transfer function is given in the subscript of Fig. 14. Because the harmonics injected into the PCC terminal are mainly the 5th, 7th, 11th and 13th harmonics, N is selected as 5, 7, 11 and 13 respectively (as shown in Fig. 14 (b), (c), (d), (e)).

As can be seen from the harmonic histogram in Fig. 14 (a), the THD of i_2 is 4.43%. Although there is no 3rd harmonic at the PCC terminal, the equivalent output impedance of the system increases around three times the frequency of the fundamental wave. Therefore, all the harmonics in this band except the 3rd harmonic are still suppressed, which is consistent with the analysis conclusion in Fig. 8.

In Fig. 14 (b), (c), (d) and (e), N selects different order of harmonics respectively, and the harmonic order corresponding to N is highlighted in red in the histogram. Obviously, with the gradual increase of N, THD gradually changes from 3.3% to 2.92%, 4.34% and 6.28%. The reason is that the main components of the harmonics injected into the PCC terminal are the 5th and 7th harmonics, while the content of the 11th and 13th harmonics is relatively small. Therefore, compared with $N=7$, the frequency band with increased impedance at $N=5$, $N=11$ and $N=13$ is far different from the harmonic band contained in the PCC terminal, and the harmonic suppression effect is poor.

When $N=7$ (as shown in Fig. 14 (c)), the THD of i_2 is 2.92%. Compared with the full feed-forward method in Fig. 13 (c), the THD is reduced by 0.92%. And the order of the differential term goes from $\lambda=2$ to $\lambda=0.1431$, the differential term becomes very weak, which avoids the over-modulation phenomenon and helps to enhance the stability of the system.

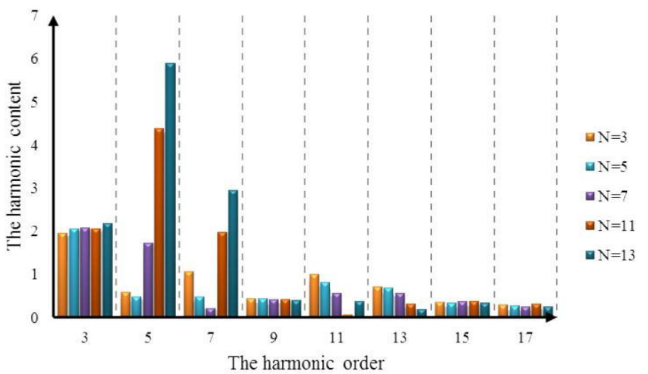

Fig. 15. *Harmonics analysis of fractional-order full feed-forward method and parameter table.*

In order to show that the theoretical derivation of this method is consistent with experimental results, the harmonic histograms in Fig. 14 are summarized and compared, as shown in Fig. 15. Obviously, in the 5th harmonic, the harmonic content is the lowest when $N=5$. Similarly, among the 7th, 11th and 13th harmonics, the harmonic content is the lowest when $N=7$, $N=11$ and $N=13$, respectively. And the 3rd and 9th harmonics content of several methods is the same, which is caused by the switch tube of the inverter in the system. The results indicate that the proposed method can accurately suppress a certain order harmonic by selecting N.

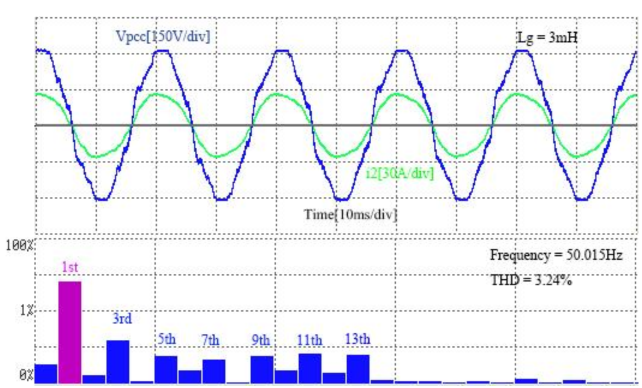

(a) L_g=3mH

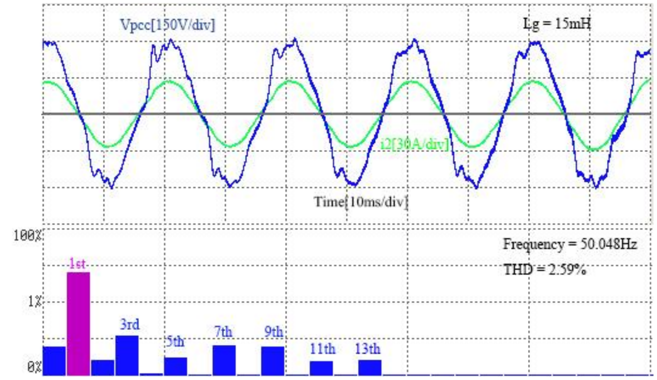

(b) L_g=15mH

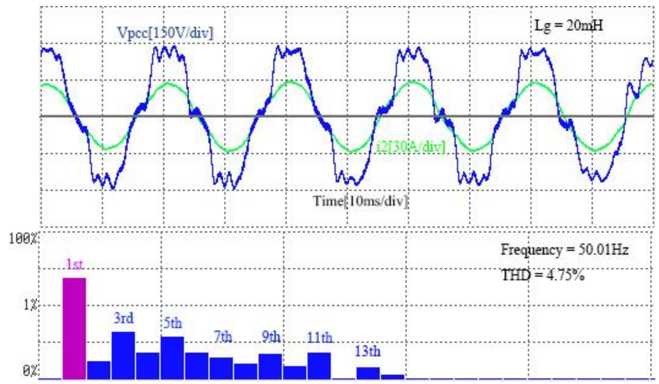

(c) L_g=20mH

Fig. 16. *Grid-connected voltage-current waveform and current harmonic analysis of the proposed method in the case of L_g changes.*

The experimental results in Fig. 16 proof the effectiveness of the proposed method and its influence on the stability of the system under the condition of L_g changes. When L_g=3mH, the THD of i_2 is 3.24%. With the further increase of L_g, the distortion of v_{pcc} is gradually serious, and the phase-locked angle is distorted, which leads to poor grid-connected power quality. When L_g=15mH, the waveform of v_{pcc} gets worse, but the THD droop to 2.59%, this is because the increase of L_g further suppresses the harmonics of i_2, and the proposed method effectively suppresses the interference of v_{pcc}. When L_g=20mH, it can be seen that the system still maintains stable operation and the THD is 4.75% in the case of v_{pcc} distortion worse than that at L_g=15mH. Therefore, the proposed method has good harmonic suppression performance and stability in the case of L_g changes, which is consistent with the analysis of control performance and system stability in Section 3.

It can be seen from Table 3 that, the differential-order in the mathematical model of the three traditional feed-forward methods (Type1, Type2 and Type3) is directly related to the control performance. With the increase of the order of the differential term, the effective frequency band of harmonic suppression increases continuously. Although the full feed-forward method has a good harmonic suppression effect, it is difficult to realize the higher-order differential term in its mathematical model in engineering, and it is sensitive to noise, which easily makes the system in the over-modulation state, resulting in poor stability of the system.

Table 3 Performance comparison table of different feed-forward methods

	Type 1	**Type 2**	**Type 3**	**The proposed method**
The order of the differential term	0	1	1,2	<1
The complexity of the implementation	simple	medium	difficult	difficult
The suppression effect of harmonics	poor	general	good	good
Sensitivity to noise perturbation	small	medium	large	small

Different from the three traditional feed-forward methods mentioned above, although the implementation difficulty of this method is increased, the proposed method successfully reduces the differential order of feed-forward term on the basis of further suppressing the harmonics of the system. Therefore, the method is insensitive to noise, the system is in the normal modulation process, and has good stability.

Table 4 Performance comparison table of different harmonic suppression methods

Harmonic suppression method	location	Parameter design	Implementation complexity	Harmonic suppression effect
The proposed method	Feedforward branch	simple	difficult	excellent
PR+HR controller	current loop	difficult	difficult	general

In engineering, PR+HR controller is generally used to suppress the interference of grid voltage harmonics. Table 4 shows the performance comparison between this method and the proposed method. As can be seen from Table 4, the parameter design process of PR+HR controller and the implementation process in the digital system are relatively complex, and the harmonic suppression ability is poor. However, this method has strong robustness because it directly controls the current loop.. In contrast, the proposed method is to suppress the voltage harmonics through feedforward branches. Therefore, the harmonic suppression ability is strong, and the parameter design process is simple. However, it relies heavily on parameters L_1 and C , and the implementation process is relatively complex.

V. CONCLUSION

In this paper, a novel fractional full feed-forward method of grid voltage is proposed to solve the voltage harmonic interference in the PCC terminal. Parameters of the proposed method are obtained by using vector fitting between the fractional differential term and the ideal full feed-forward transfer function. The Bode diagram of the equivalent output impedance is given to analyze the suppression ability of the proposed method, and the root locus diagram proves the effect on the stability of the system.

Experiment results show that the proposed method not only improves the grid side current quality from $THD = 3.85\%$ to $THD = 2.92\%$, but also reduces the order of differential link from $\lambda=2$ to $\lambda=0.1431$, which is more suitable for engineering implementation. On the basis of the proposed method, a feedforward control method with high harmonic suppression performance and more suitable for engineering application is the direction of our future research.

REFERENCES

[1] X. Chen, X. Ruan, D. Yang, W. Zhao and L. Jia, "Injected grid current quality improvement for a voltage-controlled grid-connected inverter", IEEE Trans. Power Electron., vol. 33, no. 2, pp. 1247-1258, Feb. 2018.

[2] X. Guo, "A novel CH5 inverter for single-phase transformerless photovoltaic system applications", IEEE Trans. Circuits Syst. II Exp. Briefs, vol. 64, no. 10, pp. 1197-1201, Oct. 2017.

[3] Lumbreras, D., et al., Trends in power quality, harmonic mitigation and standards for light and heavy industries: A Review. Energies, 2020. 13(21): p. 5792.

[4] D. Zhu, S. Zhou, X. Zou and Y. Kang, "Improved design of PLL controller for LCL-type grid-connected converter in weak grid," IEEE Transactions on Power Electronics, vol. 35, no. 5, pp. 4715-4727, May. 2020.

[5] D. Zhu, S. Zhou, X. Zou, Y. Kang and K. Zou, "Small-signal disturbance compensation control for LCL-type grid-connected converter in weak grid," IEEE Transactions on Industry Applications, vol. 56, no. 3, pp. 2852-2861, May-June. 2020.

[6] T. Liu and D. Wang, "Parallel structure fractional repetitive control for PWM inverters," in IEEE Transactions on Industrial Electronics, vol. 62, no. 8, pp. 5045-5054, Aug. 2015.

[7] K. Seifi and M. Moallem, "An adaptive PR controller for synchronizing grid-connected inverters," in IEEE Transactions on Industrial Electronics, vol. 66, no. 3, pp. 2034-2043, March. 2019.

[8] H. Komurcugil, N. Altin, S. Ozdemir and I. Sefa, "Lyapunov-function and proportional-resonant-based control strategy for single-phase grid-connected VSI with LCL filter," in IEEE Transactions on Industrial Electronics, vol. 63, no. 5, pp. 2838-2849, May. 2016.

[9] J. Selvaraj and N. A. Rahim, "Multilevel inverter for grid-connected PV system employing digital PI controller," in IEEE Transactions on Industrial Electronics, vol. 56, no. 1, pp. 149-158, Jan. 2009.

[10] M. Liserre, R. Teodorescu and F. Blaabjerg, "Multiple harmonics control for three-phase grid converter systems with the use of PI-RES current controller in a rotating frame", IEEE Trans. Power Electron., vol. 21, no. 3, pp. 836-841, May. 2006.

[11] X. Wang, X. Ruan, S. Liu and C. K. Tse, "Full feedforward of grid voltage for grid-connected inverter with LCL filter to suppress current distortion due to grid voltage harmonics", IEEE Trans. Power Electron., vol. 25, no. 12, pp. 3119-3127, Dec. 2010.

[12] Y. A.-R. I. Mohamed, "Suppression of low- and high-frequency instabilities and grid-induced disturbances in distributed generation inverters", IEEE Trans. Power Electron., vol. 26, no. 12, pp. 3790-3803, Dec. 2011.

[13] W. Li, X. Ruan, D. Pan and X. Wang, " Full-feedforward schemes of grid voltages for a three-phase LCL -type grid-connected inverter ", IEEE Trans. Ind. Electron., vol. 60, no. 6, pp. 2237-2250, Jun. 2013.

[14] D. Yang, X. Ruan and H. Wu, "Impedance shaping of the grid-connected inverter with LCL filter to improve its adaptability to the weak grid

condition", IEEE Trans. Power Electron., vol. 29, no. 11, pp. 5795-5805, Nov. 2014.

[15] J. He et al., "Deadbeat weighted average current control with corrective feed-forward compensation for microgrid converters with nonstandard LCL filter", IEEE Trans. Power Electron., vol. 32, no. 4, pp. 2661-2674, Apr. 2017.

[16] Y. Ye and Y. Xiong, "UDE-based current control strategy for LCCL-type grid-tied inverters ", IEEE Trans. Ind. Electron., vol. 65, no. 5, pp. 4061-4069, May. 2018.

[17] M. A. Hannan, Z. A. Ghani, A. Mohamed and M. N. Uddin, "Real-time testing of a fuzzy-logic-controller-based grid-connected photovoltaic inverter system," in IEEE Transactions on Industry Applications, vol. 51, no. 6, pp. 4775-4784, Nov.-Dec. 2015.

[18] X. Fu and S. Li, "Control of single-phase grid-connected converters with LCL filters using recurrent neural network and conventional control methods," in IEEE Transactions on Power Electronics, vol. 31, no. 7, pp. 5354-5364, July. 2016.

[19] S. Yang, Q. Lei, F. Z. Peng and Z. Qian, "A robust control scheme for grid-connected voltage-source inverters," in IEEE Transactions on Industrial Electronics, vol. 58, no. 1, pp. 202-212, Jan. 2011.

[20] Y. He, X. Wang, X. Ruan, D. Pan, X. Xu and F. Liu, "Capacitor-current proportional-integral positive feedback active damping for LCL-type grid-connected inverter to achieve high robustness against grid impedance variation," in IEEE Transactions on Power Electronics, vol. 34, no. 12, pp. 12423-12436, Dec. 2019.

[21] W. Zheng, Y. Luo, Y. Pi and Y. Chen, "Improved frequency-domain design method for the fractional order proportional–integral–derivative controller optimal design: a case study of permanent magnet synchronous motor speed control," in IET Control Theory & Applications, vol. 12, no. 18, pp. 2478-2487, 2018

[22] J. Fei and H. Wang, "Experimental investigation of recurrent neural network fractional-order sliding mode control of active power filter," in IEEE Transactions on Circuits and Systems II: Express Briefs, vol. 67, no. 11, pp. 2522-2526, Nov. 2020.

[23] F. M. Zaihidee, S. Mekhilef and M. Mubin, "Application of fractional order sliding mode control for speed control of permanent magnet synchronous motor," in IEEE Access, vol. 7, pp. 101765-101774, 2019.

[24] J. Viola, L. Angel and J. M. Sebastian, "Design and robust performance evaluation of a fractional order PID controller applied to a DC motor," in IEEE/CAA Journal of Automatica Sinica, vol. 4, no. 2, pp. 304-314, April. 2017.

Qingyi Wang received his Ph.D. degree in Huazhong University of Technology, Wuhan, China, in 2008. He has worked at China University of Geosciences (Wuhan) since 2008. His research interests include measurement and control systems and automation equipment, power electronic power conversion technology and control methods.

Binlei Ju received his B.E degree in electrical engineering and automation from Hefei University of Technology, China, in 2018. He is currently studying for his master’s degree in control engineering at China University of Geosciences (Wuhan). His research interests include power converter and power electronics applications in renewable energy.

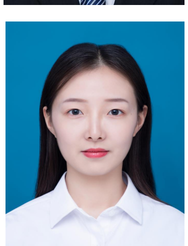

Yudi Lei received her B.E degree in electrical engineering and automation from Wuhan Polytechnic University, Wuhan, China, in 2020. She is currently studying for her master’s degree in control engineering at China University of Geosciences (Wuhan). Her research interests include hardware design and power converter.

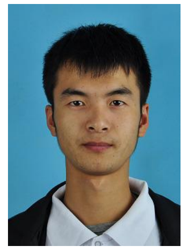

Dan Zhou graduated from China University of Geosciences (Wuhan) with a bachelor's degree. He is now studying for a master's degree in control science and engineering at the same school, majoring in intelligent perception and measurement and control technology.

Shuai Yin received his B.E degree in electrical engineering and automatic chemistry from Northeastern University of Qinhuangdao, Shenyang, China, in 2019. He is currently studying for his master’s degree in control engineering at China University of Geosciences (Wuhan). His research interests include converter fault diagnosis and fractional order PID controller.

Danyun Li received her Ph.D. degree from Central South University in 2016. She has worked at China University of Geosciences (Wuhan) since 2016. Her research interests include control and optimization of wind power generation system, power electronics and electric drives.